Research Report

Light Manipulation with Dielectric Gratings

Hideo Iizuka, Nader Engheta, Hisayoshi Fujikawa, Kazuo Sato and Yasuhiko Takeda

Report received on Jun. 26, 2012

ABSTRACT Gratings have periodic structures composed of ridges and grooves and provide a unique feature of discrete angles in diffraction phenomenon. Gratings are among the key devices in optics and photonics with the growth of nanofabrication technologies. Here we review two functional gratings in our recent theoretical works. The first one is a grating coupler that efficiently diffracts the normal incident light into the +1st-order diffraction with a large refraction angle such as 50°. The second one is a double-sided grating switch with the horizontal shift that provides a relatively wide bandwidth due to the non-resonance operation. The modal analysis provides physical insights for such unique diffraction phenomena.

KEYWORDS Diffraction, Gratings, Optics, Periodic Structures, Photonics

1. Introduction

Gratings have periodic structures composed of ridges and grooves and are among the key devices in optics and photonics with the growth of nanofabrication technologies. Gratings have been investigated for not only fundamental building blocks such as filters[1-3] and resonators[4] but also applications of displays[5] and solar cells.[6,7] Also, asymmetry in the grating structure can provide a specific diffraction order coupling that is called "blazed grating".[8-12] An experimental work in 2000[8] showed an aspect ratio of ~12 for TiO_2 grating ridges and a recent progress in nanofabrication technologies for gratings is seen in Ref. (13). With regard to analytical methods for gratings, the modal analysis[14-17] provides physical insights for diffraction phenomena with the mode behaviors, while the rigorous coupled mode analysis[18,19] has an advantage of being suitable for various ridge shapes such as semi-circle, triangular, and curved surfaces.

Here we review two functional gratings in our recent theoretical works. In Section 2, a grating coupler[20] is presented. It is generally challenging to efficiently couple the normal incident light into the +1st-order diffraction with a large diffraction angle. To the best of our knowledge the largest +1st-order diffraction angle has so far been ~25° reported in Ref. (8). The double-groove grating we present has a large refraction angle of 50°. In Section 3, a double-sided grating switch with the horizontal shift[21] is presented. In Ref. (22), a transmission filter has been reported that can tune a resonance peak with the horizontal movement of the top and bottom gratings. The double-sided grating switch we present shows a relatively wide bandwidth due to the non-resonance operation.

2. Grating Coupler with a Large Refraction Angle of 50°

Figure 1(a) shows the configuration of a TiO_2 double-groove grating attached on top of a semi-infinite SiO_2 substrate. The grating has two grooves

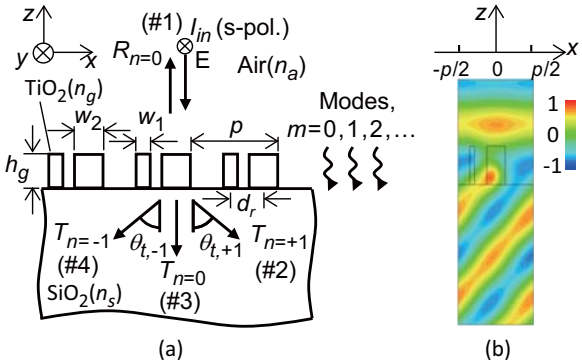

Fig. 1 (a) Configuration of the double-groove grating. (dimensions; p = 540 nm, w_1 = 35 nm, w_2 = 130 nm, d_r = 170 nm, & h_g = 280 nm, refractive index; n_a = 1, n_s = 1.45, & n_g = 2.38, and +1st / –1st-order diffraction angle; $\theta_{t,+1} = \theta_{t,-1}$ = 50° at 600 nm operating wavelength) (b) snap shot of electric field distribution at 600 nm obtained by the CST Microwave Studio™ simulation.

with two different widths per period. For the normally incident s-polarized light, three propagating and other evanescent modes are excited along the z axis in the grating. Selecting the grating period of p = 540 nm, the +1st / –1st-order diffraction angle is set at 50° at a design wavelength of λ_0 = 600 nm. This angle is larger than the critical angle of 43.6° at the SiO_2-air interface. A grating refractive index of n_g = 2.38, ridge widths of w_1 = 35 nm and w_2 = 130 nm, and their distance of d_r = 170 nm are selected to excite three propagating modes with large enough amplitudes to be enhanced or suppressed at the grating end. A grating height of h_g = 280 nm is chosen such that these three modes are simultaneously in-phase for the +1st order, but out-of-phase for the –1st- and 0th-orders, at the grating end. This provides the coupling of the incident light mainly into the +1st-order transmission. This is observed in the snap shot (in time) of the electric field distribution that was simulated by the Finite-Integration-Technique-based simulator, CST Microwave Studio™,[23] as shown in Fig. 1(b). Both the simulation and the modal analysis results show 96.9% efficiency for the +1st-oder diffraction.

Propagating modes in the grating are investigated by the modal analysis. **Figure 2**(a) shows the equivalent circuit. The inset shows the three orthogonal mode profiles (m is the mode number and is assigned from the largest eigenvalue) where the amplitudes are normalized to unity at $x = w_2 / 2$ (wider ridge edge). The coupling coefficient $C_{m,n}$ from the mth mode to the nth order transmission[20] is introduced. Lack of symmetry in the structure over one period allows $C_{m,n}$ to have different phases but the same amplitude for $-n$ and $+n$ at normal incidence. Figures 2(b)-(d) show $C_{m,n}$ in the complex plane for each diffraction order. Eleven modes were included in the calculation. $C_{m,n=+1}$ has nearly the same phase for m = 0, 1, and 2, resulting in the summation enhancement for n = +1 (Fig. 2(b)). While the same amplitude but the different phase of $C_{m,n=-1}$ suppresses the summation for n = –1 (Fig. 2(d)). The summation for n = 0 is also suppressed (Fig. 2(c)). Diffraction characteristics of this grating are inherently not sensitive to changes in the operating wavelength, incidence angle, and dimensions due to the non-resonance operation.

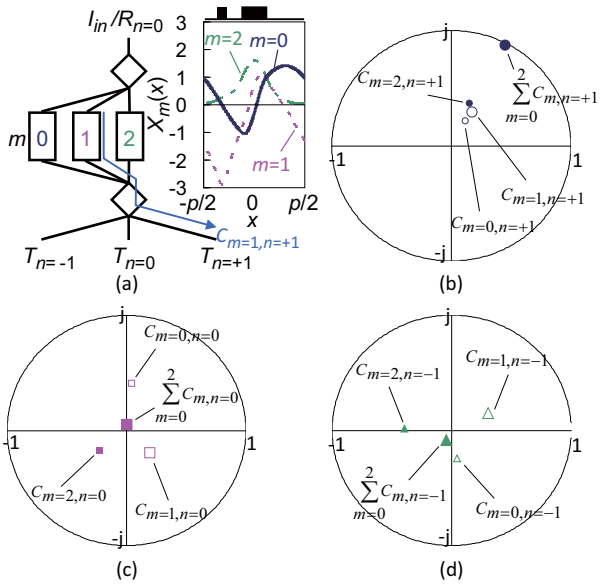

Fig. 2 (a) Equivalent circuit and coupling coefficients for (b) n = +1, (c) n = 0, & (d) n = –1 obtained from the modal analysis.

Table 1 shows the scattering parameters obtained using the modal analysis. For each input port most of the power exits mainly from one of the four ports. **Figures 3**(a)-(d) show the electric field amplitude distributions for four possible devices. The double-groove grating is used in these four devices except for the input port of Fig. 3(b). In our simulations, a 5-μm-width incident light source with approximately flat amplitude and phase distributions is utilized. The incident light after passing through the grating A is trapped into the SiO_2 substrate ($|S_{21}|$ = 96.9%, as shown in Table 1) and is exited at the grating B ($|S_{12}|$ = 96.9%), via the two bounces, as shown in Fig. 3 (a). Figure 3(b) shows a beam splitter with the parallel in/out light. The light is split into the +1st / –1st-orders with a 50° angle at the regular grating C that is shown in **Fig. 4**(a), and is exited at each grating D and E ($|S_{12}|$ = 96.9%). Another interesting feature of this grating is an isolation characteristic that leads to a reflector, as shown in Fig. 3(c). The trapped light inside the substrate via the grating F is diffracted at the grating G into the $+z$ direction ($|S_{34}|$ = 83.1%). The light is

Table 1 Scattering parameters at 600 nm when the grating is regarded as a four-port device.

Incidence Port	Diffraction efficiency at each port #1	#2	#3	#4
#1	1.9%	96.9%	0.3%	0.9%
#2	96.9%	1.9%	1.2%	0.0%
#3	0.3%	1.2%	15.4%	83.1%
#4	0.9%	0.0%	83.1%	16.0%

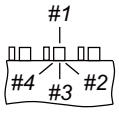

diffracted at the grating H ($|S_{43}|$ = 83.1%) again and propagates to the $-x$ direction with several bounces. It must be noted that the light is reflected by sandwiching the substrate with the top and bottom gratings, due to the isolations ($|S_{24}|$ = 0.0%) at G and ($|S_{23}|$ = 1.2%) at H. Inserting the grating L ($|S_{12}|$ = 96.9%) into the reflector of Fig. 3(c) provides a light delay device as shown in Fig. 3(d). Transmission efficiencies of 93.9%, 96.1%, and 64.8% are estimated for the three devices in Fig. 3(a), (b), and (d) from Table 1 when the plane wave incidence is assumed and multi-reflections are not considered. $|S_{43}|$ and $|S_{34}|$ are maximized to 93.1% by optimizing dimensions, and the estimated efficiency is increased from 64.8% to 81.4% for Fig. 3(d).

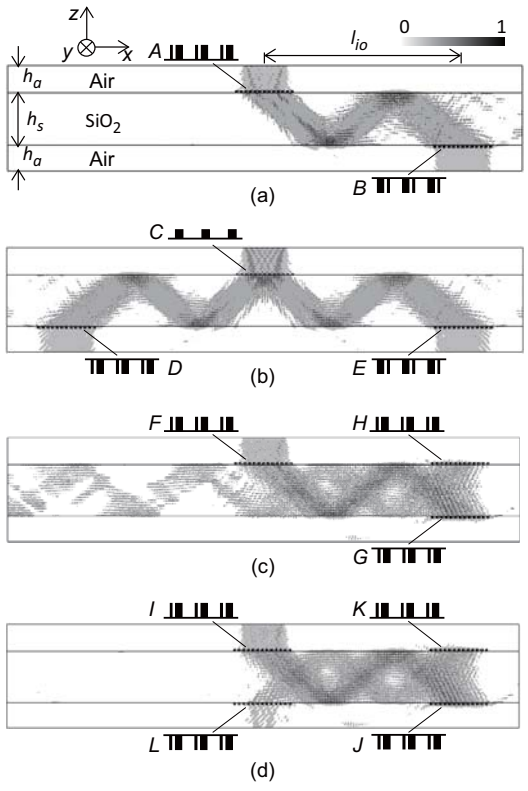

Fig. 3 Simulation results for the electric field amplitude distributions at 600 nm for (a) coupler, (b) parallel beam splitter, (c) reflector, and (d) delay device. A 5-μm-width incident light source is located at h_a = 3 μm away from the input grating. Transmission efficiencies with 7-μm-width ports at h_a = 3 μm away from output gratings are 72%, 74.4%, and 36.7% for three devices (a), (b), and (d). Each grating has a 13 period length. (other dimensions; h_s = 6 μm & l_{io} = 23 μm)

3. Double-sided Grating Switch with Horizontal Shift

Figure 4(a) shows the configuration of the TiO_2 grating beam splitter attached on top of a semi-infinite SiO_2 layer. Two propagating (m = 0 & 1) and other evanescent ($m \geq 2$) modes are excited along the z axis in the grating when the normally incident s-polarized light is illuminated upon the TiO_2 grating. The grating is designed as a beam splitter by coupling the incident wave mainly into the –1st / +1st-order transmission diffraction (n = –1 & +1) with the suppression of the 0th-order diffraction (n = 0). Selecting the grating period of p = 540 nm, the –1st / +1st refraction angle is set at 50° at the design wavelength of λ_0 = 600 nm. The SiO_2 layer supports the 0th and –1st / +1st propagating (n = –1, 0, & +1) and other evanescent ($n \geq 2$) diffraction orders in the operating wavelength range of 500 nm to 700 nm, while the air region has the 0th and –1st / +1st propagating diffraction orders (n = –1, 0, & +1) from 500 nm to 540 nm, and only the 0th propagating diffraction order (n = 0) from 540 nm

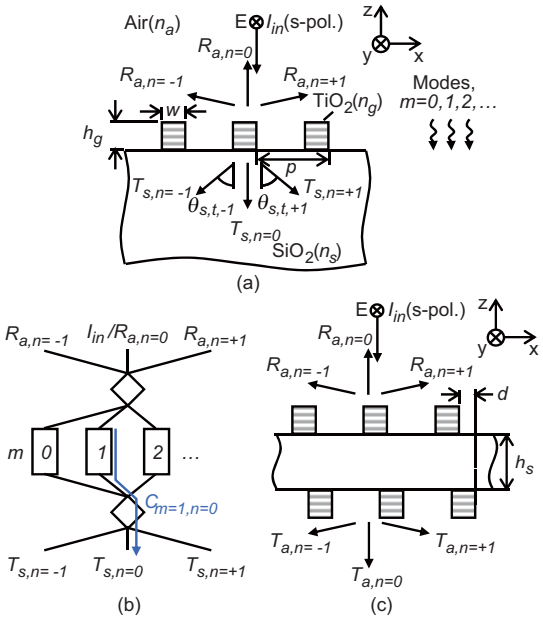

Fig. 4 (a) Configuration and (b) equivalent circuit of the grating "beam splitter". (dimensions; p = 540 nm, w = 145 nm, & h_g = 175 nm, refractive index; n_a =1, n_s =1.45, & n_g = 2.38, and –1st /+1st refraction angle; $\theta_{s,t,-1} = \theta_{s,t,+1}$ = 50° at λ_0 = 600 nm) (c) configuration of double-sided grating with the switching capability. (interlayer thickness; h_s = 260 nm, and grating dimensions; same as Fig. 4(a))

to 700 nm. The grating refractive index, $n_g = 2.38$, and the ridge width, $w = 145$ nm, are selected to excite two propagating modes ($m = 0$ & 1) with equal amplitudes in the grating. The grating height, h_g = 175 nm, corresponding to the propagation length of the mode, is chosen such that these two modes are out-of-phase at the grating's end. These result in the suppression of the 0th-order transmission diffraction (n = 0). Figure 4(b) shows the equivalent circuit with coupling coefficient $C_{m,n}$ for such modes. The double-sided grating consists of the SiO_2 interlayer sandwiched between the two identical gratings as shown in Fig. 4(c). The top and bottom gratings may be shifted horizontally by the distance, d.

The refractive index of the grating, n_g, has an important role to play in the functionality of this grating as a beam splitter. **Figure 5**(a) shows diffraction efficiency as a function of n_g at 600 nm. Eleven modes were included in the calculation. The grating height, h_g, and the ridge width, w, were adjusted to maximize the –1st / +1st-order diffraction

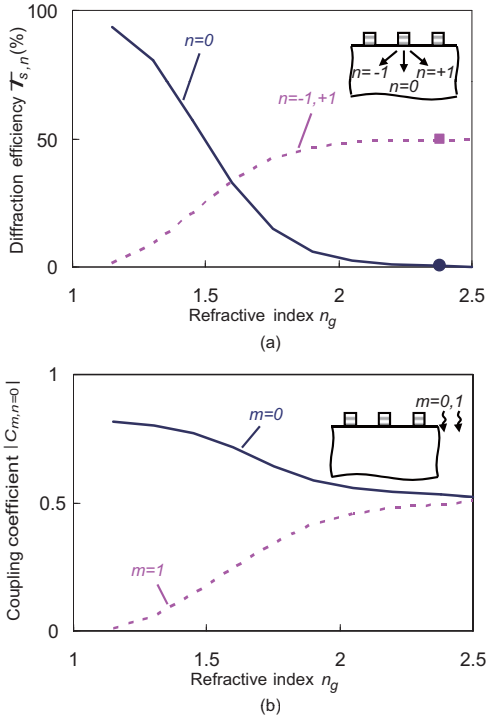

Fig. 5 (a) Diffraction efficiency and (b) coupling coefficient of the grating beam splitter as a function of refractive index of grating at 600 nm operating wavelength. (Solid line and dashed line are obtained using the modal analysis. The single dots (shown as a "circle" and a "square") are the results of the CST Microwave Studio™ simulation.)

at each n_g. As n_g is increased, the –1st / +1st-order diffraction efficiency ($n = -1$ & +1) is increased while the 0th-order diffraction efficiency ($n = 0$) is decreased. Diffraction efficiency gives a –1st / +1st-order transmission efficiency of 49.6% for each, with the 0th-order suppressed to 0.5% at $n_g = 2.38$. The results of the numerical investigation by CST Microwave Studio™ agree well with those by the modal analysis. This beam splitter characteristic of the TiO_2 grating can be understood in Fig. 5(b) for $C_{m,n}$. Not only is $m = 0$ mode present, but also $m = 1$ mode is excited as n_g is increased. When the both modes are excited with equal amplitudes, the out-of-phase condition cancels out the 0th-order transmission diffraction (n = 0) as the appropriate grating height, h_g is used.

Figures 6(a)-(d) show the snap shot (in time) of the electric field distributions at 600 nm for four cases. In case of the semi-infinite SiO_2 layer in Fig. 4(a), each of the –1st / +1st-order diffracted light propagates toward the –50° / +50° direction in the SiO_2 layer (i.e., in-phase along the dashed line AA' for +50°) due to the splitting of the incident light as shown in Fig. 6(a). There are alternating "plus" and "minus" peaks (i.e., standing wave) along the x direction (i.e., the dotted line BB'). As we see in Fig.6(a), the peaks of this standing wave in the SiO_2 layer happen at $x = -p / 2$, 0, and $+p / 2$. This implies that nulls (i.e., the zero) of

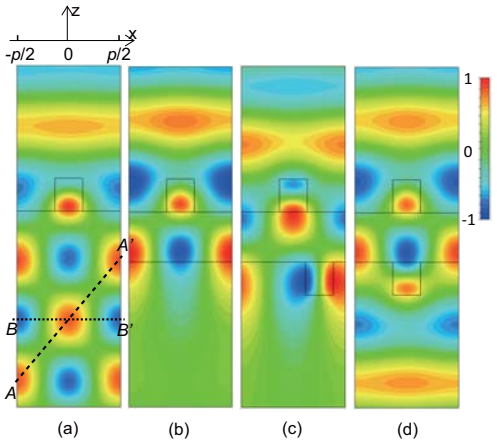

Fig. 6 Snap shot (in time) of the electric field distributions at 600 nm operating wavelength. The electric field is normalized to the maximum value in each figure. (a) The SiO_2 layer with the top grating has the semi-infinite thickness. (b) The SiO_2 interlayer with the top grating has a finite thickness of $h_s = 260$ nm. The top and bottom gratings have (c) the shift of a quarter period, and (d) no shift in the horizontal direction.

electric field are at $x = -p / 4$ and $+p / 4$. This peak/zero electric field distribution is the key point in the light coupling/decoupling phenomena between the top and bottom gratings in our proposed structure. Incident light reflects back at the bottom of SiO_2-air interface when the SiO_2 interlayer has a thickness of 260 nm, as shown in Fig. 6(b). The interesting feature is that the incident light reflects back even when the bottom grating is attached with the horizontal shift of $d = p / 4$, as shown in Fig. 6(c). The top grating provides the electric field peaks at $x = -p / 2$, 0, and $+p / 2$ that correspond to the zero electric field regions for the bottom grating when shifted by $d = p / 4$, resulting in light decoupling. It is worth noting that this phenomenon happens only in the case of the grating acting as a beam splitter with a refraction angle larger than the critical angle of the SiO_2-air interface. Figure 6(d) shows the case of no shift, where light goes through with the 0th-order transmission, since both the top and bottom gratings have the electric field peaks at $x = -p / 2$, 0, and $+p / 2$.

Figure 7 shows the characteristics of the switching capability of the double-sided grating structure. The transmittance of the 0th-order diffraction ($n = 0$) is less than 5% from 552 nm to 654 nm at the horizontal shift of $d = p / 4$, while it is larger than 95% from 553 nm to 670 nm with no shift, i.e., $d = 0$. This results in switching capability in the wavelength range of 553 nm to 654 nm, exhibiting a relatively wide bandwidth (16.7%) due to the non-resonance operation. The range of switching is bounded by the resonances at the shorter and longer wavelengths. Between 500 nm and 540 nm, the incident light couples to the –1st / +1st-order diffraction rather than to the 0th-order diffraction for $d = p / 4$, while the –1st / +1st-order diffraction is much smaller than the 0th-order diffraction for $d = 0$.

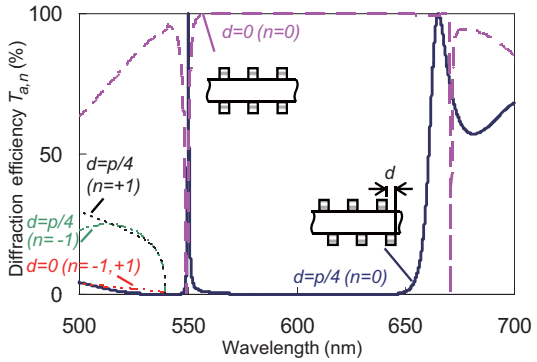

Fig. 7 Diffraction efficiency of the transmission in the double-sided grating for the quarter-period shift and no shift.

4. Conclusions

A grating coupler and grating switch have been reviewed. The unique diffraction phenomena have been well described by the modal analysis exploring mode behaviors. Potential applications of the grating coupler include a light guided window where a laser beam couples in/out at any point of the window. The grating switch can be used in a variety of scenarios and applications such as lasers, the light emitting diodes and the window shutter for sun light illumination control with unpolarized designs. Moreover, the decoupling phenomenon at both top and bottom gratings may also provide a helpful method for improving the efficiency in detectors and solar cells collecting light at both sides.

References

(1) Magnusson, R. and Wang, S. S., "New Principle for Optical Filters," *Appl. Phys. Lett.*, Vol.61, No.9 (1992), pp.1022-1024.
(2) Brundrett, D. L., Glytsis, E. N. and Gaylord, T. K., "Normal-incidence Guided-mode Resonant Grating Filters: Design and Experimental Demonstration," *Opt. Lett.*, Vol.23, No.9 (1998), pp.700-702.
(3) Ding Y. and Magnusson, R., "Doubly Resonant Single-layer Bandpass Optical Filters," *Opt. Lett.*, Vol.29, No.10 (2004), pp.1135-1137.
(4) Bruckner, F., Friedrich, D., Clausnitzer, T., Burmeister, O., Britzger, M., Kley, E. B., Danzmann, K., Tunnermann, A. and Schnabel, R., "Demonstration of a Cavity Coupler Based on a Resonant Waveguide Grating," *Opt. Express*, Vol.17, No.1 (2009), pp.163-169.
(5) Magnusson, R. and Shokooh-Saremi, M., "Widely Tunable Guided-mode Resonance Nanoelectromechanical RGB Pixels," *Opt. Express*, Vol.15, No.17 (2007), pp.10903-10910.
(6) Eisele, C., Nebel, C. E. and Stutzman, M., "Periodic Light Coupler Gratings in Amorphous Thin Film Solar Cells," *J. Appl. Phys.*, Vol.89, No.12 (2001), pp.7722-7726.
(7) Zaidi, S. H., Gee, J. M. and Ruby, D. S., "Diffraction Grating Structures in Solar Cells," *Proc. 28th IEEE Photo. Spec. Conf.*, (2000), pp.395-398.
(8) Lee, M. S. L., Lalanne, P., Rodier, J. C. and

Cambril, E., "Wide-field-angle Behavior of Blazed-binary Gratings in the Resonance Domain," *Opt. Lett.*, Vol.25, No.23 (2000), pp.1690-1692.
(9) Oliva, M., Michaelis, D., Benkenstein, T., Dunkel, J., Harzendorf, T., Matthes, A. and Zeitner, U. D., "Highly Efficient Three-level Blazed Grating in the Resonance Domain," *Opt. Lett.*, Vol.35, No.16 (2010), pp.2774-2776.
(10) Lalanne, P., Astilean, S., Chavel, P., Cambril, E. and Launois, H., "Blazed Binary Subwavelength Gratings with Efficiencies Larger than Those of Conventional Echelette Gratings," *Opt. Lett.*, Vol.23, No.14 (1998), pp.1081-1083.
(11) Astilean, S., Lalanne, P., Chavel, P., Cambril, E. and Launois, H., "High-efficiency Subwavelength Diffractive Element Patterned in a High-refractive-index Material for 633 nm," *Opt. Lett.*, Vol.23, No.7 (1998), pp.552-554.
(12) Lalanne, P., Astilean, S., Chavel, P., Cambril, E. and Launois, H., "Design and Fabrication of Blazed Binary Diffractive Elements with Sampling Periods Smaller than the Structural Cutoff," *J. Opt. Soc. Am. A*, Vol.16, No.5 (1999), pp.1143-1156.
(13) Lim, S. H., Saifullah, M. S. M., Hussain, H., Loh, W. W. and Low, H. Y., "Direct Imprinting of High Resolution TiO_2 Nanostructures," *Nanotechnology*, 21 (2010), 285303.
(14) Sheng, P., Stepleman, R. S. and Sanda, P. N., "Exact Eigenfunctions for Square-wave Gratings: Application to Diffraction and Surface-plasmon Calculations," *Phys. Rev. B*, Vol.26, No.6 (1982), pp.2907-2917.
(15) Clausnitzer, T., Kampfe, T., Kley, E.-B., Tunnermann, A., Peschel, U., Tishchenko, A. V. and Parriaux, O., "An Intelligible Explanation of Highly-efficient Diffraction in Deep Dielectric Rectangular Transmission Gratings," *Opt. Express*, Vol.13, No.26 (2005), pp.10448-10456.
(16) Feng, J., Zhou, C., Zheng, J. and Wang, B., "Modal Analysis of Deep-etched Low-contrast Two-port Beam Splitter Grating," *Opt. Commun.*, Vol.281 (2008), pp.5298-5301.
(17) Iizuka, H., Engheta, N., Fujikawa, H. and Sato, K., "Incident Angle Dependency of Propagating Modes in Rectangular Grating for Polarization-independent −1st Order Diffraction or Polarization Splitting," *Micro. Opt. Tech. Lett.*, Vol.52, No.6 (2010), pp.1362-1369.
(18) Yokomori, K., "Dielectric Surface-relief Gratings with High Diffraction Efficiency," *Appl. Opt.*, Vol.23, No.14 (1984), pp. 2303-2310.
(19) Gerritsen, H. J. and Jepsen, M. L., "Rectangular Surface-relief Transmission Gratings with a Very Large First-order Diffraction Efficiency (95%) for Unpolarized Light," *Appl. Opt.*, Vol.37, No.25 (1998), pp.5823-5829.
(20) Iizuka, H., Engheta, N., Fujikawa, H., Sato, K. and Takeda, Y., "Role of Propagating Modes in a Double-groove Grating with a +1st-order Diffraction Angle Larger than the Substrate-air Critical Angle," *Opt. Lett.*, Vol.35, No.23 (2010), pp.3973-3975.
(21) Iizuka, H., Engheta, N., Fujikawa, H., Sato, K. and Takeda, Y.,"Switching Capability of Double-sided Grating with Horizontal Shift," *Appl. Phys. Lett.*, Vol. 97 (2010), 053108.
(22) Nakagawa, W. and Fainman, Y., "Tunable Optical Nanocavity Based on Modulation of Near-field Coupling between Subwavelength Periodic Nanostructures," *IEEE J. Select. Topics Quantum Electron.*, Vol.10, No.3 (2004), pp.478-483.
(23) CST Microwave Studio 2009, <http://www.cst.com/Content/Products/MWS/Overview.aspx>, (accessed 2012-07-26).

Hideo Iizuka

Research Field:
- Electromagnetic Analysis

Academic Degree: Dr.Eng.
Academic Societies:
- IEEE
- OSA
- The Institute of Electronics, Information and Communication Engineers

Awards:
- IEICE Young Eng. Award, 2001

Nader Engheta*

Research Fields:
- Electromagnetics
- Metamaterials
- Plasmonics Optics
- Microwave, Nanophotonics and Nano-optics, Nanoantennas

Academic Degree: Ph.D
Academic Societies:
- IEEE
- OSA
- APS
- SPIE
- IOP
- Sigma Xi
- MRS
- Union Radio-Scientifique Internationale
- American Association for the Advancement of Science

Awards:
- IEEE Electromagnetics Award, 2012
- Selected in Scientific American Magazine List of Top 50 Leaders in Science and Technology, 2006
- Fellow of IEEE, APS, SPIE, OSA, and American Association for the Advancement of Science

*University of Pennsylvania

Hisayoshi Fujikawa

Research Field:
- Functional Thin Film Devices

Academic Degree: Dr.Eng.
Academic Societies:
- The Japan Society of Applied Physics
- The Optical Society of Japan

Kazuo Sato

Research Field:
- Mobile Antennas

Academic Degree: Dr.Eng.
Academic Societies:
- IEEE
- The Institute of Electronics, Information and Communication Engineers

Yasuhiko Takeda

Research Fields:
- Solar Cells
- Optical and Transport Properties of Nanostructured Materials

Academic Degree: Dr.Eng.
Academic Society:
- The Japan Society of Applied Physics

Awards:
- R&D 100 Awards, 2000
- Best Poster Award of Renewable Energy, 2006
- The 20 Highest Scored Abstracts of the 27th European Photovoltaic Solar Energy Conference, 2012

